Available online at www.sciencedirect.com
SCIENCE DIRECT
Surface & Coatings Technology 191 (2005) 255–262
SURFACE & COATINGS TECHNOLOGY
www.elsevier.com/locate/surfcoat

Low-temperature nitriding of stainless steel in an electron beam generated plasma

C. Muratore*[,1], D. Leonhardt, S.G. Walton, D.D. Blackwell[2], R.F. Fernsler, R.A. Meger

Plasma Physics Division, Naval Research Laboratory, 4555 Overlook Ave S.W., Washington, DC 20375-5346, USA

Received 30 October 2003; accepted in revised form 16 February 2004
Available online 10 May 2004

Abstract

An electron beam generated plasma processing system was characterized with in situ diagnostics and employed for a series of low energy (350 eV) stainless steel nitriding experiments in the temperature range of 325–462 °C. Plasma characterization yielded quantitative ion specie fluxes to the stainless steel workpiece in an argon–nitrogen plasma, with a significant fraction of the flux comprised of N^+ ions. The nitriding rates were as high as 20 μm $h^{-1/2}$ with surface layers exhibiting hardness values of approximately 15.5 GPa for specimens processed at all temperatures. X-ray diffraction analysis revealed nitrogen concentrations of approximately 30 at.% in all samples processed below 460 °C. The process activation energy was comparable to that in nitriding systems with higher ion fluxes, suggesting favorable plasma chemistry with respect to plasma nitriding applications.
© 2004 Elsevier B.V. All rights reserved.

Keywords: Plasma generation; Nitriding; Nano-identation; X-ray diffraction

1. Introduction

Low-temperature plasma nitriding processes incorporating remote plasma sources have been investigated by different groups as industrially viable means of nitriding austenitic stainless steel [1–4]. Maintenance of low workpiece temperature during nitriding is necessary to maintain the corrosion resistance associated with AISI 316 and other grades of stainless steel, which is reported to decrease significantly at temperatures in excess of 450 °C due to precipitation of chromium nitride [5]. Czerwiec et al. [4] point out that the standard industrial practice of dc glow discharge nitriding, in which the workpieces constitute the plasma cathode, is less useful for nitriding materials with properties that are sensitive to processing temperature because the discharge current can result in unpredictable heating of the workpiece over time. Additionally, when nitriding large areas, large power supplies must be used to sustain the discharge at the required voltage. Decoupling plasma production from the substrate also allows for independent control of the ion flux and incident ion energy, thus plasma generation independent of the workpieces is desirable, and is a common theme in the development of new nitriding process technologies. The most useful remotely generated nitriding plasma would contain high concentrations of chemically active nitrogen species uniformly distributed over a large area with minimal power consumption [6–9].

Multiple kilovolt electron beams passing through a 1–65 Pa nitrogen gas background generate plasmas that have demonstrated ion densities between 10^{10} and 10^{12} cm^{-3}, and are capable of delivering large atomic ion fluxes [10,11]. Beam generated plasmas also require less input power per electron-ion pair than most other plasma generation techniques that rely upon discharges driven by electric fields. Furthermore, most of the energy supplied by the electron beam is consumed by gas ionization and dissociation reactions rather than by electron heating and gas excitation as in conventional sources [12], resulting in a low plasma electron temperature (~0.5 eV). Additionally, plasmas generated by electron beams are easily scalable to large areas and a variety of geometries [13]. Uniform planar plasmas of approximately one square meter are routinely generated with electron beams in the Large Area Plasma

* Corresponding author. Tel.: +1-202-404-5754; fax: +1-202-767-3553.
E-mail address: cmurator@ccs.nrl.navy.mil (C. Muratore).
[1] NRL/ASEE Postdoctoral Research Fellow.
[2] SFA, Largo, MD 20744, USA.

0257-8972/$ - see front matter © 2004 Elsevier B.V. All rights reserved.
doi:10.1016/j.surfcoat.2004.02.026

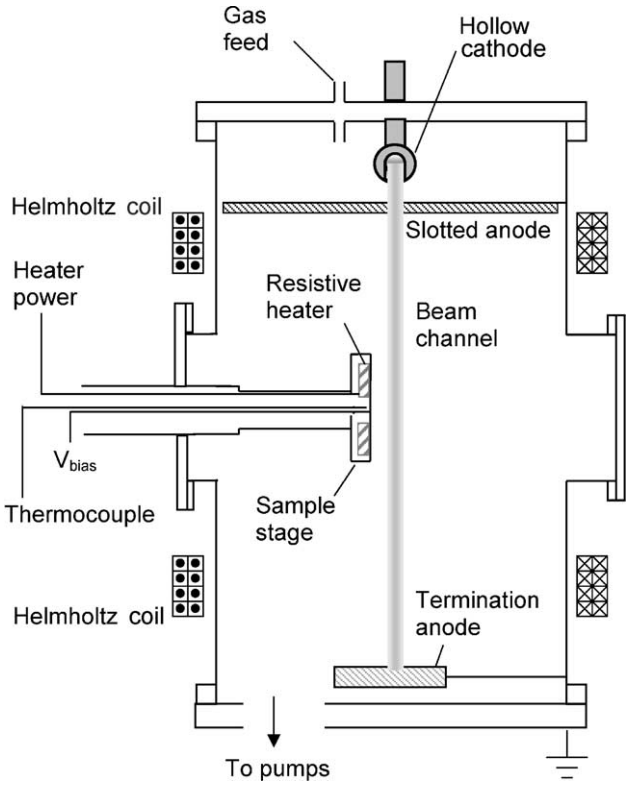

Fig. 1. Schematic of the processing chamber.

Processing Systems (LAPPS) developed at the US Naval Research Laboratory.

To investigate the utility of electron beam generated plasmas for plasma-assisted nitriding applications, argon–nitrogen plasmas were produced with a 2 keV, pulsed, planar electron beam and characterized using a mass spectrometer and an electrostatic probe. Samples of AISI 316 stainless steel were then nitrided under identical plasma conditions at temperatures between 325 and 462 °C. The nitrided specimens were characterized using optical microscopy, X-ray diffraction, and nanoindentation techniques.

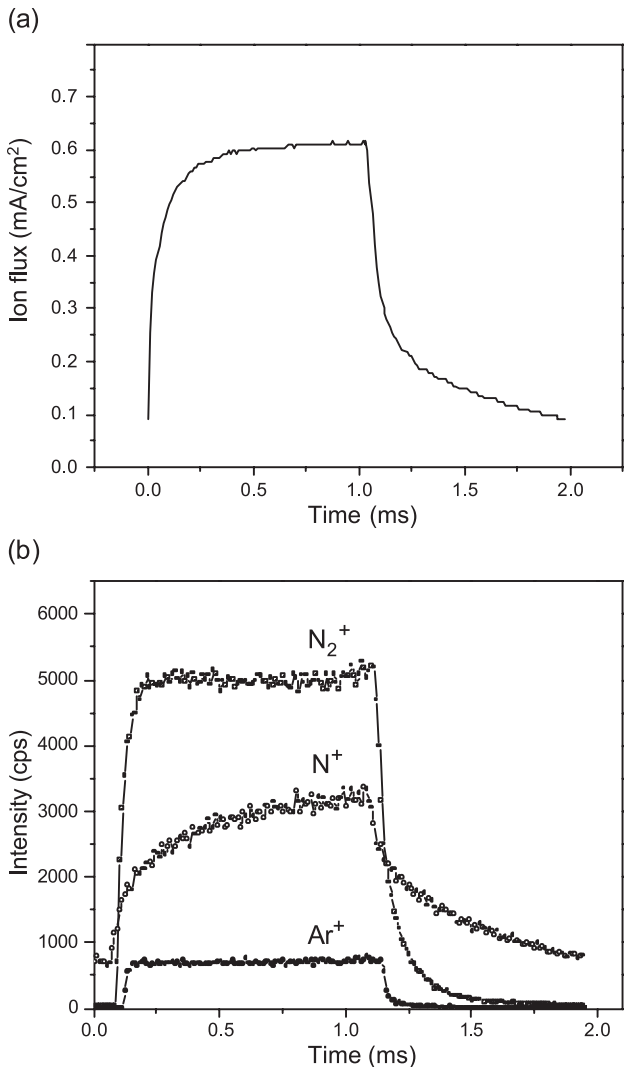

Fig. 2. The total (a) and relative (b) ion flux incident on the substrate during the cathode pulse.

2. Experimental procedure

Fig. 1 illustrates the processing chamber fitted with an electrically isolated sample stage designed to allow heating and biasing of the specimens to be nitrided, which was also used for quantitative ion flux measurements. Additional plasma characterization experiments were performed with a Hiden Analytical Limited electrostatic quadrupole plasma (EQP) energy and mass analyzer for determination of the relative N_2^+, N^+ and Ar^+ ion fluxes in a similar system described in detail elsewhere [11]. The front electrode of the EQP was located approximately 1 cm from the edge of the beam channel as in the nitriding experiments, but was maintained at ground potential. The EQP output was monitored using a 10 μs scanning gate synchronized to the high voltage cathode pulse to obtain time resolution [14].

For all plasma characterization and processing experiments, the base pressure was 1×10^{-4} Pa or lower, and gases

Table 1
Process parameters for all nitriding experiments

Substrate bias (−V)	Pressure (Pa)	Gas mixture (%)	Cathode frequency (Hz)	Pulse duration (ms)	Duty factor (%)	Elapsed time (h)	Exposure time (h)
350	21.3	80N_2/20Ar	500	1	50	7	3.5

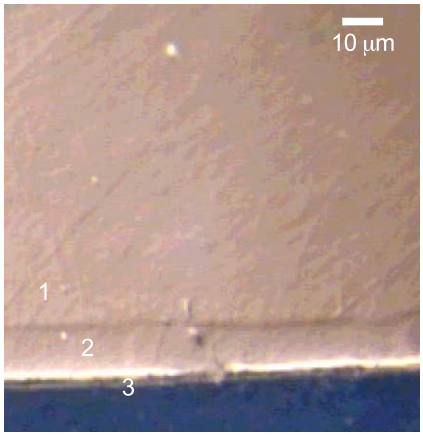

Fig. 3. Cross-sectional optical micrographs of AISI 316 steel substrates processed at 415 °C, under the conditions specified in Table 1. There are three visibly distinct regions: (1) the substrate, (2) the nitrided region, and (3) a metal film deposited to preserve the edge of the nitrided layer.

of at least 99.999% purity were introduced via variable leak valves. A 15-cm-long linear hollow cathode was driven by a 1 ms, −2 kV pulse at 500 Hz, and the resultant electron beam was collimated by a 165 G magnetic field parallel to the electron beam path. The beam passed through a 15×1 cm wide slot in a grounded plate (slotted anode) and passed through the chamber to a termination anode positioned normal to the direction of the beam approximately 60 cm from the hollow cathode. The average current delivered to the cathode during the pulse was 50 mA as measured with a current pulse transformer (Pearson Electronics, Model 110), resulting in a total power of 100 W to the cathode during the pulse.

Samples of 0.6 cm thick, electropolished AISI 316 stainless steel with an average surface roughness of approximately 0.020 μm were used for all nitriding experiments. X-ray diffraction was employed prior to nitriding to insure that the surface of each substrate was free of stress-induced martensite, which has been shown to inhibit growth of the expanded austenite (γ_N) phase in austenitic stainless steel [15,16]. The samples were degreased ultrasonically in separate acetone and methanol baths, then loaded in the vacuum chamber and pumped down to base pressure. The chamber was pressurized to 21.3 Pa with a mixture of 88% nitrogen and 12% argon, and the plasma was initiated. All samples were dc biased to −350 V, and heated to the processing temperature within 30 min. The substrates were then maintained at a constant temperature while exposed to the plasma, which was pulsed at 50% duty, for an additional 6.5 h. The total exposure time of the substrate to the plasma, including the 30 min heating phase of the process (50% of 7.0 h), was used to calculate the nitriding rate. To obtain accurate temperature measurements, an electrically isolated thermocouple imbedded in the substrate holder was calibrated with respect to a thermocouple that was spot welded to the surface of a sacrificial substrate subject to both heating and ion bombardment. Over the course of each experiment the sample was held within 5 °C of the reported temperature. All samples were allowed to cool naturally in 20 Pa nitrogen to room temperature before venting the vacuum chamber. A summary of the processing parameters is provided in Table 1.

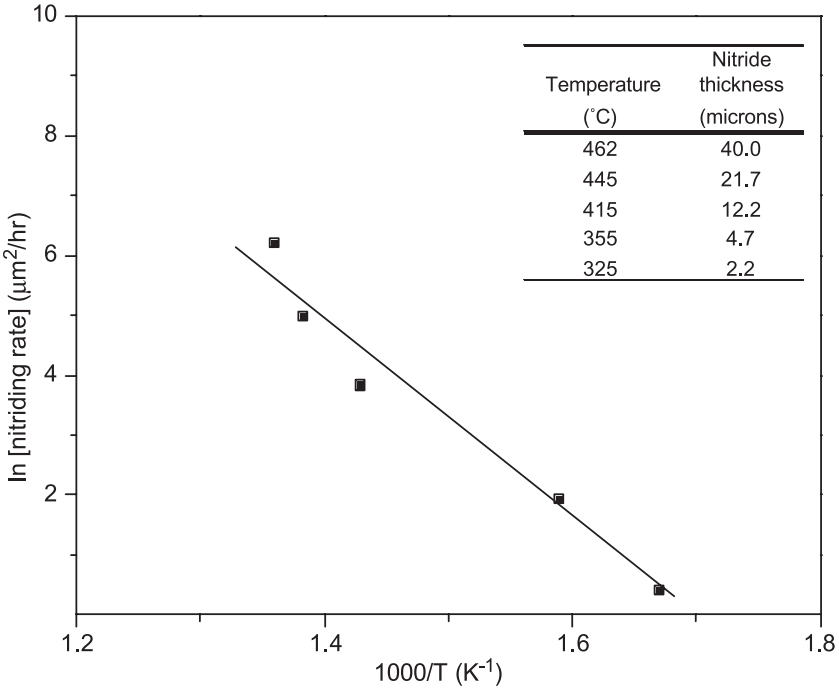

Fig. 4. Arrhenius style plot of the temperature dependent rate data (inset). The line is a least squared fit to the data.

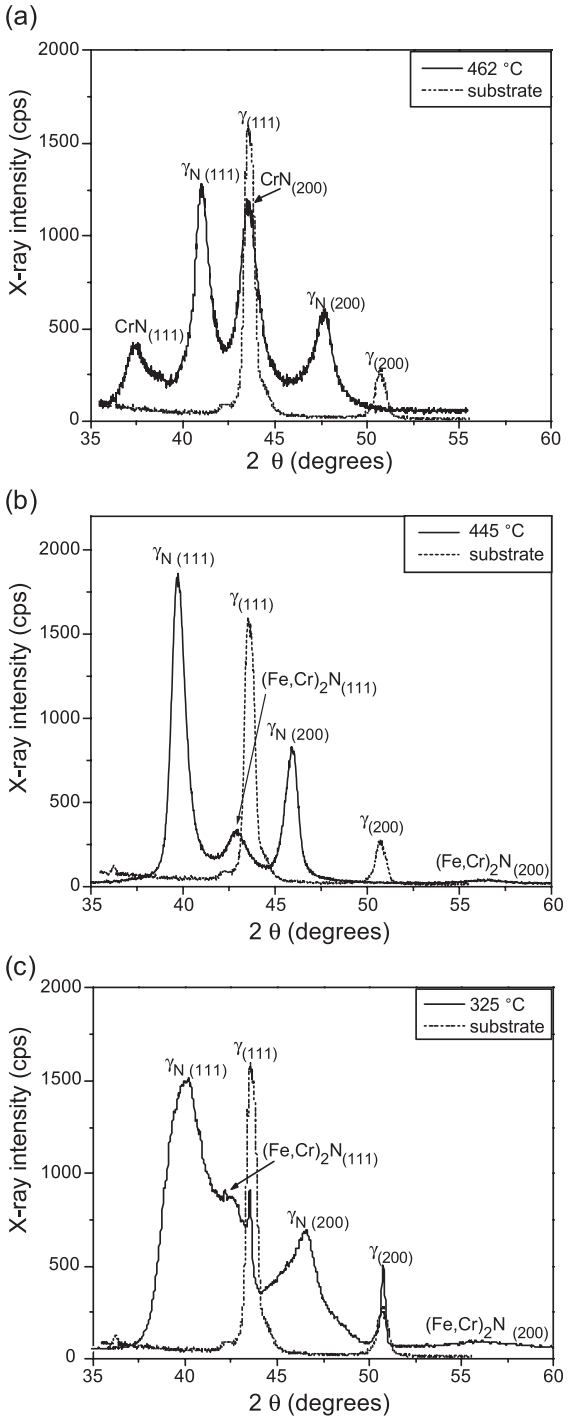

Fig. 5. Bragg–Brentano X-ray diffractograms for nitrided surfaces processed at (a) 462 °C, (b) 445 °C and (c) 325 °C.

The nitrided specimens were sectioned and sputter coated with a thin layer of titanium to protect the nitrided surface during metallographic preparation. The sample was maintained at room temperature during metal deposition. Each cross section was polished to 1 μm by hand and etched in Marble's solution for 10 s, and then repolished to 1 μm. The cross sections were observed in an optical microscope to obtain the nitride layer thickness, which was measured to approximately 0.2 μm precision with the cursors of a Vickers microindenter. The X-ray diffractograms presented here were obtained in a Rigaku 15 kW X-ray diffractometer using Cu K_α radiation operated in the Bragg–Brentano configuration. An Ultra Micro Indentation System 2000 (UMIS) fitted with a Berkovich diamond indenter was used to characterize hardness of sample surfaces and cross sections.

3. Results

3.1. Plasma characterization

Fig. 2a shows the total positive ion flux (assuming negligible secondary electron emission) collected at the workpiece biased to −350 V averaged over 200 cathode periods. The ion flux decayed to less than 25% of its maximum value of 0.6 mA cm^{-2} 400 μs into the plasma afterglow. Fig. 2b shows the time- and mass-resolved ion flux over a cathode period, where the atomic ions exhibited a long decay time compared to the molecular nitrogen ions. Note that the offset from zero on the time axis in Fig. 2b was due to the time-of-flight of each specie in the EQP. Integration of the mass-resolved ion fluxes showed that the total ion flux was approximately 55% molecular nitrogen ions, 40% atomic nitrogen ions, with the balance comprised of argon ions.

3.2. Materials characterization

Fig. 3 shows a cross section of the sample nitrided at 415 °C, as observed in the optical microscope. The depths of the nitride layers for samples processed at temperatures between 325 and 462 °C are tabulated and plotted in an Arrhenius-type plot in Fig. 4. X-ray diffractograms for specimens processed at different temperatures are plotted with the unprocessed substrate diffraction pattern in Fig. 5a–c. The appearance of an fcc phase, analogous with the substrate but with increased lattice spacing, appears as a result of the nitriding treatment. The X-ray diffraction patterns at all temperatures were consistent with the presence of a supersaturated fcc iron–nitrogen solid solution, or expanded austenite (γ_N) phase as reported by other workers in AISI 316 and other grades of stainless steel [4,15–17]. The total lattice strain in the AISI 316 substrate exhibited weak dependence on orientation as shown in Table 2, in agree-

Table 2
Lattice strains and calculated percentages of nitrogen based on lattice expansion from the measured equilibrium value of 3.597 nm

Temperature (°C)	$a\ \gamma_{N(111)}$ (nm)	$a\ \gamma_{N(200)}$ (nm)	$\Delta d/d_o$ (111) (%)	$\Delta d/d_o$ (200) (%)	$C_{N(avg)}$ (at.%)
462	3.811	3.806	5.9	5.8	21
445	3.929	3.948	9.2	9.8	30
325	3.890	3.894	8.1	8.3	27

ment with Fewell et al. [18]. The effect of residual compressive stress on lattice expansion was calculated using the methodology outlined by Öztürk et al. [19], where the maximum possible compressive stress (σ) was assumed to be equivalent to the approximate yield strength of the nitrided material (2 GPa), and the lattice parameter of the expanded austenite $a(\gamma_N)$ was given by,

$$a(\gamma_N) = a + 2S_1 a\sigma,$$

where S_1 is the (hkl) dependent X-ray elastic constant and a is the lattice constant of the material strained only by the presence of interstitial nitrogen atoms. The contribution of stress to lattice expansion was less than 1% for every sample. It was therefore assumed that the measured lattice distortion was entirely due to a 7.2×10^{-4} nm expansion per nterstitial N atom among 100 substrate atoms, as reported by Cheng et al. [20]. The nitrogen contents at the same depth relative to the surface for the (111) and (200) oriented γ_N grains averaged together for selected samples are reported in Table 2, and were approximately 30% for samples processed at temperatures of 445 °C or less. Additionally, the $(Fe,Cr)_2N$ phase was apparent in all samples with the exception of the nitride layer formed at 462 °C. This phase has been observed by others [21,22] at the surface of the nitrided layer in similar stainless steel alloys processed in the same temperature range. No evidence of CrN formation was present in samples processed at temperatures less than 450 °C, suggesting that the temperature measurements of the substrate during processing were not overestimated.

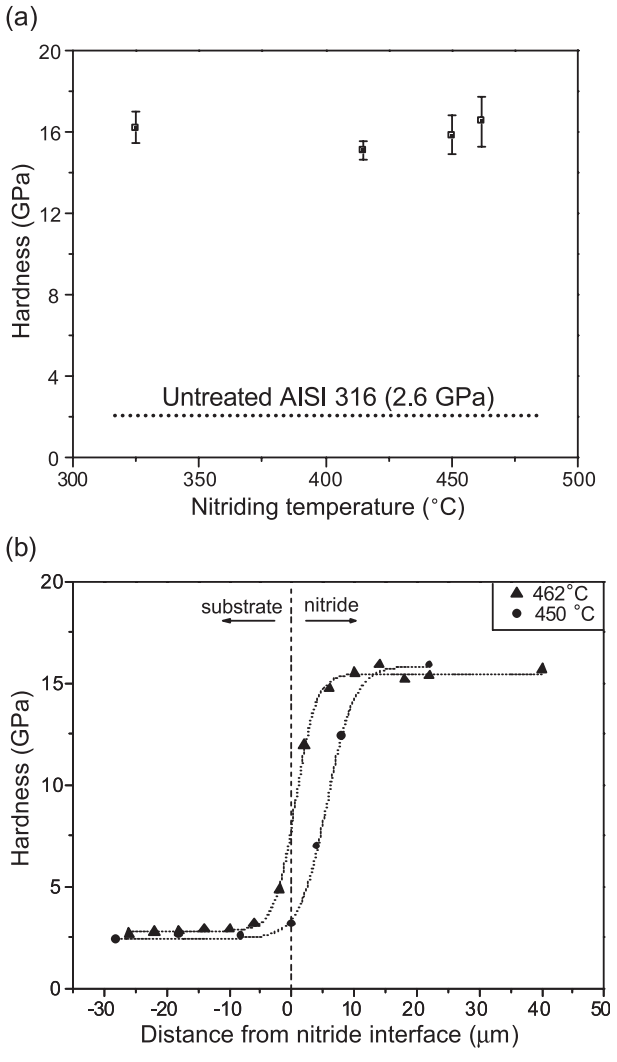

Fig. 6. Hardness values measured (a) at the surface of samples processed at the indicated temperature and (b) over the cross section near the surface of the two thickest nitride layers.

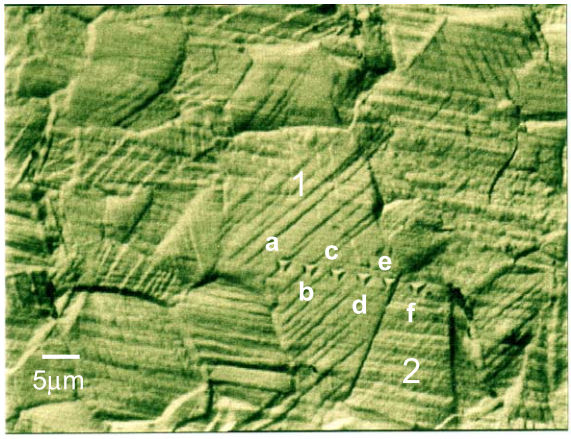

Indent	Hardness (GPa)	Indent location
a	13.3	fissure, grain 1
b	14.1	fissure, grain 1
c	17.2	featureless region, grain 1
d	17.0	featureless region, grain 1
e	17.1	featureless region, grain 1
f	16.0	featureless region, grain 2

Fig. 7. Optical micrograph of the surface of the sample processed at 415 °C after indentation. The labeled indents correspond to the locations and hardness values indicated in the chart above.

Values of surface hardness measured for selected samples are shown in Fig. 6a. The average of eight surface indents in random locations resulted in an average hardness of approximately 15.5 GPa±4% for all samples; however, variations of up to ±15% on individual samples were observed. Hardness values measured along the cross section of the two thickest nitrided layers (processed at 462 and 445 °C) are shown in Fig. 6b. Fig. 7 shows the surface of the sample nitrided at 415 °C, with the hardness values that correspond to each labeled indentation.

4. Discussion

4.1. Plasma characterization

Table 3 illustrates plasma nitriding rates for AISI 316 stainless steel in other plasma sources at the indicated

Table 3
A sample of parameters associated with plasma assisted nitriding processes found in the literature, including the present work

Process	Substrate temperature (°C)	Maximum ion energy (eV)	Total pressure (Pa)	Gas mixture (%)	Ion current (mA cm^{-2})	Nitriding rate (μm $h^{-1/2}$)	Reference
rf plasma	400	250	0.4	100% N_2	–	1.2	[6]
dc diode	350	2000	5.0	80N_2/20 H_2	2.00	1.8	[19]
ion beam	400	700	0.04	100% N_2	2.00	4.8	[17]
IPAP	400	1000	6.7	80N_2/20 Ar	0.75	5.5	[23]
TAT	420	500	1.0	25N_2/75 H_2	"high"	6.3	[24]
e-beam	415	350	21.3	88N_2/12 Ar	0.55	6.5	current work

All values pertain to AISI 316 stainless steel. The nitriding rate was determined by fitting the thickness and time data reported in the specified reference to a parabola with vertex at (t=0, d=0). The calculated thickness value at t=1 h is reported below for each process.

temperatures. Nitriding in electron beam generated plasmas was considerably faster than in dc glow discharge nitriding processes reported in the literature, and competitive with alternative nitriding processes with much higher ion fluxes at the substrate and approximately equivalent processing temperatures. As specified earlier, the exposure time (duty factor×total process time) was considered when calculating the nitriding rate since the plasma was pulsed. If the total processing time (7.0 h) is used in the rate calculation, the result of 5 μm $h^{-1/2}$ is still competitive with other nitriding systems.

The high rate is likely related to the relative concentrations of species in the plasma [6–9,25]. Fig. 2b shows that a significant fraction of the ion flux is atomic nitrogen. The magnitude of the flux of atomic nitrogen ions is significant, because the charge exchange cross section for the molecular nitrogen ion is large at 350 V ($Q_{ce} \approx 27\times 10^{-16}$ cm^2) compared to the momentum transfer cross section of the atomic nitrogen ion ($Q_m \approx 0.98\times 10^{-16}$ cm^2) [26]. A molecular nitrogen ion thus loses its energy in an average distance given by,

$$\lambda_{ce} = \frac{1}{Q_{ce} n_g},$$

where n_g is the density of the nitrogen gas [27a]. In 19 Pa nitrogen (88% of 21.3 Pa), the mean free path of an N_2^+ ion accelerated across the plasma sheath is 0.07 cm, while the mean free path (for momentum transfer) of N^+ ions is 1.80 cm. The sheath thickness in centimeters (s) can be estimated by:

$$s = 740\left[\frac{2(V_b)}{n_s}\right]^{1/2},$$

where V_b is the bias voltage in volts and n_s is the ion density at the sheath edge [27b] in cm^{-3}. Assuming $n_s \sim 10^{10}$ cm^{-3} and an electron temperature of 0.4 eV [10], the sheath thickness is approximately 0.2 cm—roughly three times the N_2^+ ion mean free path. Thus, for the nitriding conditions employed in this work, the kinetic energy of most molecular ions arriving at the substrate was likely reduced relative to the bias potential due to collisions in the sheath. By contrast, most of the atomic ions should have impinged upon the substrate surface with the full sheath potential—approximately 350 eV. These calculations illustrate the potential importance of atomic nitrogen ions in nitriding experiments conducted under similar conditions of gas pressure and workpiece bias. For example, sputtering to eliminate surface oxide layers during nitriding of stainless steel in high vacuum systems has been identified as a critical surface process [28,29]. TRIM simulations show that the sputter yield of oxygen in Fe_2O_3 by nitrogen ions is very sensitive to the ion kinetic energy below 350 eV. Additionally, energetic ($E_i \geq 100$ eV) nitrogen ions have a significantly increased adsorption probability compared to lower-energy nitrogen ions on similar surfaces [30].

Radical production in electron beam generated plasmas is not reported in this work, but for a multi-kilovolt electron beam the cross section for nitrogen dissociation is comparable to the ionization cross section [12]. Also, the rate constant for dissociative recombination of the molecular ion,

$$e + N_2^+ \rightarrow 2N,$$

is large ($\sim 10^{-7}$ cm^3 s^{-1} when T_e=0.4) [31]. The reaction results in rapid decay of the N_2^+ ion in the plasma afterglow compared to the atomic ion (both shown in Fig. 2a). The large dissociative rate constant results in a high probability of conversion of a beam-produced N_2^+ ion into a pair of N atoms. Several researchers have reported that neutral atomic nitrogen flux at the surface promotes nitride formation in steels [7,9,32]. Note that the dissociative recombination reaction also results in the rapid decay of the N_2^+ ions in the plasma afterglow in contrast to N^+ ions, (both shown in Fig. 2b), which are lost at a slower rate through diffusion to surfaces in the chamber [14].

Further experiments are being conducted to better determine the role of ion and radical specie concentrations on nitriding efficiency in electron beam generated plasmas [33], but the data in the work presented here suggest that atomic ion and radical production are related to high nitriding efficiency. The electron beam generated plasma system is particularly useful for nitriding stainless steel as it can be operated at higher pressures (see Table 3) for increased atomic nitrogen production without a significant

loss of energy flux at the substrate due to ion collisions in the plasma sheath.

4.2. Materials characterization

The linearity of the data in Fig. 4 suggests that nitride layers exhibited diffusion controlled growth described by the equation:

$$\frac{d^2}{t} = D_o e^{\frac{-E_a}{kT}},$$

where d is the nitrided layer thickness, t is the exposure time, E_a is the effective activation energy for diffusion and T is the temperature. An activation energy of 1.4 eV/atom was calculated from the least-squares-fit line drawn through the data in Fig. 4. The activation energy was significantly lower than the value of 1.87 eV/atom for N diffusion in AISI 316 measured by other workers [34], again suggesting that electron beam generated plasmas are rich in active nitriding species (see Ref. [25], and references contained therein). The calculated effective diffusion coefficient of 5.7 $cm^2\ s^{-1}$ was close to that observed in an fcc stainless steel of similar composition at high temperature [35].

The source of significant (±15%) variation in the hardness of a single surface found in Fig. 6a was also investigated. Fig. 7 shows the nitrided surface of the sample processed at 415 °C. The observed grain relief was not the result of chemical etching, but was likely due to differential sputtering from grains with different orientations [36]. The indents labeled "a–e" in the figure were in the same grain, and indent "f" was in a neighboring grain. The indents a and b correlate to a lower calculated hardness than indents c, d and e. As shown in Fig. 7, indents a and b are located on fissures on the surface of the grain. Similar features have been attributed to stacking fault formation due to lattice expansion by other workers [37]. The presence of stacking faults and grains with different crystallographic orientations (thus differing nitrogen contents) [25] appeared to affect the resistance of the material to the force of the indenter, thereby affecting the calculated hardness values at nitrided stainless steel sample surfaces.

5. Conclusions

Nitrogen-based electron beam generated plasmas were analyzed by mass spectrometry, and revealed large fluxes of atomic nitrogen ions compared to those found in other plasma nitriding processes. Hard layers between 2 and 40 μm thick consisting of 316 stainless steel with approximately 30 at.% nitrogen in solution were produced by subjecting the steel to nitrogen-based electron beam generated plasmas. The nitriding rate was high (about 7 μm $h^{-1/2}$ at 415 °C) relative to several other plasma nitriding processes at typical nitriding temperatures, and efficient in terms of power consumption. The growth rate was diffusion controlled with an activation energy of approximately 1.4 eV/atom. Nitrided layers exhibited a hardness of 15.5 GPa (about 6 times that of untreated SS316) independent of process temperature. The atomic nitrogen ion and neutral flux generated by the plasma was presented as the explanation for the observed high nitriding efficiency and reduced nitrogen diffusion activation energy.

Acknowledgements

This research was supported by the Office of Naval Research. The authors are grateful to Dr. I.L. Singer at NRL for insightful discussions and allowing us to use the UMIS indentor, and Dr. S.B. Qadri at NRL for access to the X-ray diffractometer. C.M. appreciates the support of the American Society for Engineering Education.

References

[1] E.I. Meletis, S. Yan, J. Vac. Sci. Technol., A, Vac. Surf. Films 11 (1993) 25.
[2] M.K. Lei, Z.L. Zhang, J. Vac. Sci. Technol., A, Vac. Surf. Films 15 (1997) 421.
[3] M.J. Baldwin, M.P. Fewell, S.C. Haydon, S. Kumar, G.A. Collins, K.T. Short, J. Tendys, Surf. Coat. Technol. 98 (1998) 1187.
[4] T. Czerwiec, N. Renevier, H. Michel, Surf. Coat. Technol. 131 (2000) 267.
[5] Z.L. Zhang, T. Bell, Surf. Eng. 1 (1985) 131.
[6] J.M. Priest, M.J. Baldwin, M.P. Fewell, S.C. Haydon, G.A. Collins, K.T. Short, J. Tendys, Thin Solid Films 354 (1999) 113.
[7] M.J. Baldwin, S.C. Haydon, M.P. Fewell, Surf. Coat. Technol. 97 (1997) 97.
[8] T. Czerwiec, H. Michel, E. Bergmann, Surf. Coat. Technol. 108–109 (1998) 182.
[9] G. Henrion, R. Hugon, M. Fabry, V. Scherentz, Surf. Coat. Technol. 97 (1997) 729.
[10] D. Leonhardt, S.G. Walton, D.D. Blackwell, W.E. Amatucci, D.P. Murphy, R.F. Fernsler, R.A. Meger, J. Vac. Sci. Technol. 19 (2001) 1367.
[11] S.G. Walton, C. Muratore, D. Leonhardt, R.F. Fernsler, D.D. Blackwell, R.A. Meger, submitted to Surface Coatings and Technology (PBII 2003 Conference Proceedings).
[12] R.F. Fernsler, W.M. Manheimer, R.A. Meger, J. Mathew, D.P. Murphy, R.E. Pechacek, J.A. Gregor, Phys. Plasmas 5 (1998) 2137.
[13] R.A. Meger, D.D. Blackwell, R.F. Fernsler, M. Lampe, D. Leonhardt, W.M. Manheimer, D.P. Murphy, S.G. Walton, Phys. Plasmas 8 (2001) 2558.
[14] S.G. Walton, D. Leonhardt, D.D. Blackwell, R.F. Fernsler, D.P. Murphy, R.A. Meger, Phys. Rev., E Stat. Phys. Plasmas Fluids Relat. Interdiscip. Topics 65 (2002) 046412.
[15] R.G. Vardiman, I.L. Singer, Mater. Lett. 2 (1983) 150.
[16] Z. Yu, X. Xu, L. Wang, J. Qiang, Z. Hei, Surf. Coat. Technol. 153 (2002) 125.
[17] D.L. Williamson, J.A. Davis, P.J. Wilbur, Surf. Coat. Technol. 103–104 (1998) 178.
[18] M.P. Fewell, D.R.G. Mitchell, J.M. Priest, K.T. Short, G.A. Collins, Surf. Coat. Technol. 131 (2000) 300.
[19] O. Öztürk, D.L. Williamson, J. Appl. Phys. 77 (1995) 3839–3850.
[20] L. Cheng, A. Böttger, Th.H. de Keijser, E.J. Mittemeijer, Scr. Metall. Mater. 24 (1990) 509.

[21] S.-P. Hannula, P. Nenonen, J.P. Hirvonen, Thin Solid Films 181 (1989) 343.
[22] E.I. Meletis, S. Yan, J. Vac. Sci. Technol., A, Vac. Surf. Films 11 (1993) 25.
[23] E.I. Meletis, Surf. Coat. Technol. 149 (2002) 95.
[24] A. Leyland, D.B. Lewis, P.R. Stevenson, A. Matthews, Surf. Coat. Technol. 62 (1993) 608.
[25] D.L. Williamson, O. Ozturk, R. Wei, P.J. Wilbur, Surf. Coat. Technol. 65 (1994) 15.
[26] A.V. Phelps, J. Phys. Chem. Ref. Data 20 (1991) 557.
[27] (a) M.A. Lieberman, A.J. Lichtenberg, Principles of Plasma Discharges and Materials Processing, Wiley, New York, 1994, p. 46;
(b) M.A. Lieberman, A.J. Lichtenberg, Principles of Plasma Discharges and Materials Processing, Wiley, New York, 1994, p. 164.
[28] M.P. Fewell, J.M. Priest, M.J. Baldwin, G.A. Collins, K.T. Short, Surf. Coat. Technol. 131 (2000) 284.
[29] S. Parascandola, O. Kruse, E. Richter, W. Moeller, J. Vac. Sci. Technol., B 17 (1999) 855.
[30] H.F. Winters, D.E. Horne, E.E. Donaldson, J. Chem. Phys. 41 (1964) 2766.
[31] F.J. Mehr, M.A. Biondi, Phys. Rev. 181 (1969) 264.
[32] G.C. Tibbetts, J. Appl. Phys. 45 (1974) 5072.
[33] C. Muratore, S.G. Walton, D. Leonhardt, R.F. Fernsler, D.D. Blackwell, R.A. Meger, J. Vac. Sci. Technol. (2004) (In press).
[34] J. Hirovonen, A. Anttila, Appl. Phys. Lett. 46 (1985) 835.
[35] A. Kuhl, D. Bergner, H.-J. Ullrich, M. Schlaubitz, P. Karduck, Mikrochim. Acta 107 (1992) 295.
[36] I.L. Singer, J. Vac. Sci. Technol. 18 (1981) 175.
[37] V. Singh, K. Marchev, C.V. Cooper, E.I. Meletis, Surf. Coat. Technol. 160 (2002) 249.